

Jan Musfeldt is Ziegler Professor of chemistry and professor of physics at the University of Tennessee in Knoxville. Yoshihiro lwasa is professor in the Quantum Phase Electronics Center and the department of applied physics at the University of Tokyo and a team leader at the RIKEN Center for Emergent Matter Science in Japan. **Reshef Tenne** is research professor emeritus at the Weizmann Institute of Science in Rehovot, Israel.







Janice L. Musfeldt, Yoshihiro

The two-dimensional materials form one- and zero-dimensional hollow structures with a host of promising mechanical, optical, and electrical properties.

ollowing the synthesis and characterization of carbon nanotubes by Sumio Iijima in 1991, researchers have been interested in synthesizing nanotubes from other single and multilayered materials besides graphene. As early as 1992, one of our groups (Tenne's) and, later on, others succeeded using boron nitride and the transition metal dichalcogenide (TMDC) compounds tungsten disulfide and molybdenum disulfide. In the past two decades, nanotubes have extended to 2D materials composed of two elements—such as metal chalcogenides, halides, and oxides—and three- or four-element misfit layered compounds.<sup>2</sup> Misfit compounds comprise alternating slabs of rock-salt structures, such as lead sulfide, and hexagonal layered compounds, such as tantalum disulfide. Given the many materials that form nanotubes in practice and in computer models, the nanostructures seem to be a genuinely stable phase of 2D materials in the nanoscale range.

A material's properties change dramatically as its dimensions are reduced. The favorable changes from bulk to two dimensions have driven interest in graphene, monolayer MoS<sub>2</sub>, and other 2D materials over the past decade. Likewise, the quasi-1D structure of nanotubes endows them with behavior that is, in some cases, entirely different from the bulk or even 2D nanostructures. A prototypical example is the WS<sub>2</sub> nanotube, which has enhanced properties, such as increased strength, photoluminescence, electron mobility, and tribological and mechanical properties. Those properties packed into nanoscale make it well suited for applications such as reinforcing polymer nanocomposites and nanoscale field-effect transistors.

Nanotubes form from inorganic 2D materials because the atoms at the edge of the material are abundant. Those edge atoms have a higher energy, and since the surface-to-volume ratio increases dramatically for nanoparticles smaller than 100 nm, it pays for the 2D nanoparticle to fold on itself and seam into a nanotubular structure or a hollow closed-cage nanoparticle, similar to fullerene. But the elastic energy per atom for folding a  $MoS_2$  or  $WS_2$  layer is about an order of magnitude larger than that for a carbon nanotube with the same

diameter. To compensate energetically, MoS<sub>2</sub> nanotubes often adopt a multiwall structure, with concentric nanotubes stabilized by van der Waals interactions. Single-wall nanotubes can thus be tricky to produce from 2D compounds.

Different strategies have been developed to synthesize inorganic nanotubes; many of them rely on high-temperature chemical syntheses. But low-temperature techniques, such as hydrothermal synthesis, have proven useful for obtaining nanotubes from many 2D materials. Only some nanotubes—for example WS<sub>2</sub>, MoS<sub>2</sub>, and BN—are produced in usable quantities. As a result, researchers have studied them, in particular WS<sub>2</sub> nanotubes, comprehensively for their unique physical properties and possible applications.

Multiwall nanotubes are complex structures. Each layer in a tube has a different diameter, number of atoms, and potentially different chirality—the lattice's orientation relative to the tube's axis. Furthermore, multiwall nanotubes in the same synthesis batch are of various diameters and lengths. That variability, and the corresponding variability in material properties, makes the study of individual tubes essential.

## Pushed to the breaking point

Individual  $WS_2$  and  $MoS_2$  nanotubes are mechanically strong. In an early experiment,  $WS_2$  nanotubes were compressed and stretched with different stresses,<sup>3</sup> as shown in figure 1a for the case of compression. A nanotube glued to a cantilever (left) would bend rather than break under severe compressive stress (center). In higher compression cases it buckled, but the nanotube still returned to its original shape when the pressure was removed. Under a large tensile stress, the nanotube's behavior depended on its diameter.  $WS_2$  nanotubes with small diameter, less than 40 nm, withstood up to 16 GPa (black triangles in the figure 1a graph). They finally broke according to the "sword in a sheath" model, in which only the outmost layer breaks and

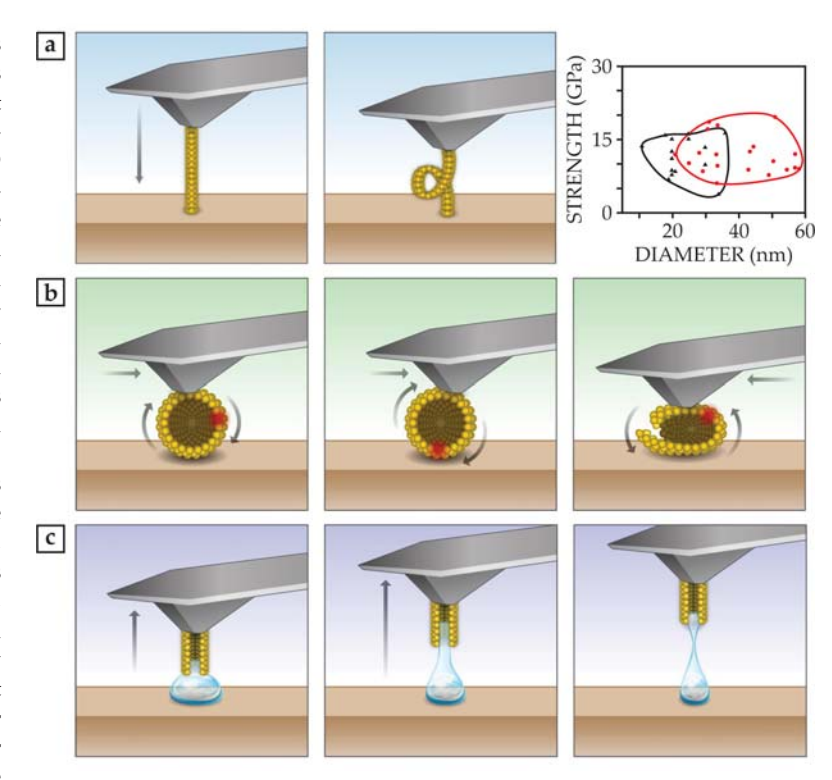


FIGURE 1. MULTIWALL TUNGSTEN DISULFIDE NANOTUBE STANDS UP TO STRESS. (a) A nanotube glued to a cantilever (left) bends when compressed (center) without any atomic deformation. The breaking point of a nanotube depends on its diameter (right), either narrow (black triangles) or larger diameter (red dots). (Adapted from ref. 3.) (b) When compressed and sheared, a nanotube rolls (left and center) until the load is high enough to cause exfoliation (right). (c) Because of strong capillary forces, inserting (left) an open-ended nanotube into the surface of a water droplet and (center) removing it draws the water into the hollow core despite the nanotube's hydrophobic surface. Even after separation (right), some water remains inside the nanotube. (Courtesy of Noa David, Weizmann Institute.)

reveals the unharmed inner tubes. On the other hand, nanotubes with larger diameter (red dots) were stronger and broke only under more than 20 GPa tensile stress. Their breakdown was through a different mechanism known as layer-by-layer, in which multiple layers share the stress and thus all break. The mechanism is possible because crystalline imperfections in larger-diameter tubes interlock the walls and allow them to share the load.

 ${
m MoS_2}$  and  ${
m WS_2}$  microparticles (platelets) have served as solid lubricants for almost 100 years. Applications include two-stroke engines, ski waxes, and bullet coatings. When the platelets are between two metal surfaces that slide past each other, the weak van der Waals interactions between the TMDC layers facilitate easy shearing of the platelets' layers and render the friction between the metal surfaces very low. In ultrahigh-vacuum conditions,  ${
m MoS_2}$  even displays vanishing friction, or superlubricity (see the article by Jean Michel Martin and Ali Erdemir, Physics Today, April 2018, page 40). But shearing is prohibited for interlocked layers in a nanotube or fullerene-like nanoparticle, as confirmed by the absence of the low-frequency

shearing Raman mode typical in bulk flakes of WS<sub>2</sub> and MoS<sub>2</sub>.

As shown in figure 1b (left and center), rolling the entire nanotube or fullerene-like nanoparticle can produce ultra-small friction coefficients, less than 0.03, even under sizable loads.4 And although the friction is comparable to that of platelets, the nanotubes last longer. For loads beyond about 0.5 GPa, the nanotube layers start flaking off (right). Those mechanically exfoliated layers settle on the metal surface, where they reduce the friction between the cantilever and the surface. Although the exact behavior in real systems is more complex, exfoliation is also the dominant failure mechanism for TMDC nanoparticles<sup>5</sup> under loads greater than 0.5 GPa but not under loads below 1 MPa, which are typical for lubricants in medical devices, such as endoscopes or catheters (see the article by Sabrina Jahn and Jacob Klein, Physics Today, April 2018, page 48). Because of their low friction, fullerene-like WS2 nanoparticles have already been used in the heavy metal industry, mining, and heavy-duty machines as solid-state lubricants and in metal working fluids.

How WS, nanotubes interact with different gases and liquids is important for applications currently under development, including artificial membranes, sensors, and polymer nanocomposites. To study those interactions, researchers dipped a single nanotube attached to a cantilever tip in and out of water,6 as shown in figure 1c. Because the W-S bonds are highly covalent and therefore highly nonpolar, the bottom rim of the nanotube is hydrophobic, and that provides a small force, which drives only a few water molecules on the tube's outer surface. Despite the minimal wetting of the outside, environmental scanning electron microscopy, atomic force microscopy experiments, and molecular dynamic calculations revealed that a receding nanotube pulls the water up with it. Capillarity forces elicit strong interactions between the water droplet and the open-ended nanotube. The nanotube's withdrawal from the water surface leads to the formation of a meniscus (figure 1c center) and

subsequent necking of the water (right). On the other hand, closed-end WS, nanotubes, which usually have diameters larger than 60 nm, were barely wetted and interacted only weakly with the water surface.6

### Vibrational insight

Raman modes, such as the one shown in figure 2a, provide additional understanding of the breakdown process of nanotubes.<sup>7</sup> When a nanotube is compressed, all its vibrational modes increase in frequency as the surrounding pressure increases (see figure 2b). However, one mode, the A<sub>1e</sub>, blueshifts at twice the rate of the others. It is an out-of-plane vibration of the chalcogen atoms (yellow spheres), and in a nanotube, the A<sub>10</sub> is a radial vibration. The mode's sensitivity to the tube's breakdown suggests that the strain passes between the tube walls through their expanding and contracting against each other. That  $A_{1g}$ mediated breakdown mechanism explains why fractures are generally perpendicular to the tube's axis, as shown in the transmission electron microscopy (TEM) images of the tubes before and after compression in figure 2c.7

Strained WS<sub>2</sub> nanotubes show the opposite trend. Raman scattering on a stretched nanotube embedded in polymer fibers revealed redshifting of the mode frequencies, which indicated load transfer. 8,9 In the future, using tip-enhanced spectroscopic techniques, researchers should be able to employ that systematic frequency shift to test for local strain in isolated WS, tubes under a load.

Raman scattering is a useful tool for uncovering the properties of TMDCs in general. In the 1970s the breathing and shear vibrations of entire layers were an early indication of the 2D layered structure of bulk TMDCs,10 and various Ramanactive modes are used today to quantify a crystal's quality and the thickness of exfoliated few- and single-layer flakes. Recent theoretical work suggests that, just as in TMDC flakes, the

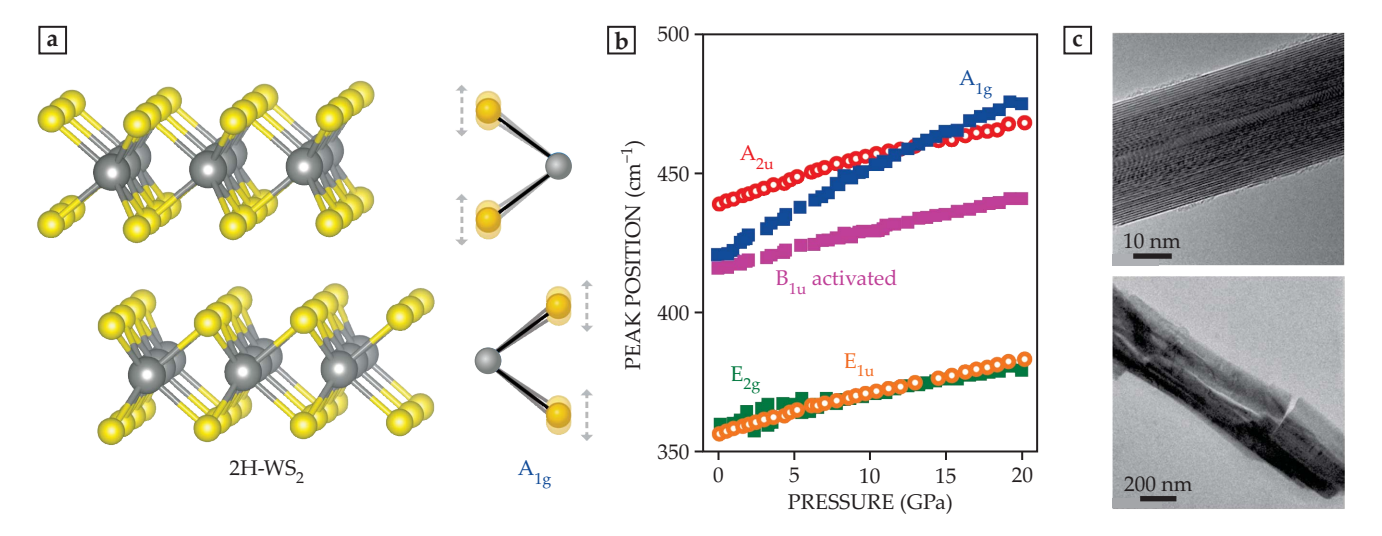


FIGURE 2. THE VIBRATIONAL PROPERTIES OF MULTIWALL NANOTUBES change under compression. (a) Each layer of tungsten disulfide has a layer of W (gray spheres) sandwiched between two layers of S (yellow). One of the possible Raman modes,  $A_{10}$ , is an out-of-plane vibration of the S atoms and a radial motion in the nanotube. (b) All of the nanotube's vibrational modes (A<sub>1g</sub>, A<sub>2u</sub>, B<sub>1u</sub>, E<sub>2g</sub>, and E<sub>1u</sub>) increase in frequency (peak position) as the pressure increases. The  $A_{1g}$  mode is more sensitive to compression, and it blueshifts at twice the rate of the others. (c) A pristine nanotube, shown in the upper transmission electron microscopy image, is damaged (lower image) after compression at 20 GPa. The tube fractures perpendicular to its axis, and the outer layer exfoliates. (Adapted from ref. 7.)

vibrations of MoS<sub>2</sub> tubes—that is, their phonons—can be a sensitive probe of crystallinity and morphology.<sup>10</sup> Raman and IR mode frequencies, symmetries, and selection rules may distinguish the tube diameter and chirality, such as zigzag or armchair chiralities.<sup>11</sup>

Phonons can also be in resonance with electronic excitations. Nanotubes have different bound states of electrons and holes, or excitons, and Raman modes with certain symmetries exchange energy with certain excitons. For

example, the odd-symmetry  $B_{\rm 1u}$  mode, which is activated by disorder,  $^{\rm 12}$  resonates with what is known as the A exciton, whereas only the  $A_{\rm 1g}$  mode resonates with a different exciton known as the B exciton.

### Mind the gap

Bulk TMDCs, such as MoS<sub>2</sub> and WS<sub>2</sub>, are indirect gap semiconductors, which means a charge carrier moving from the valence to the conduction band requires phonon assistance. When reduced to a monolayer, MoS2 acquires a direct gap, and thus strong photoluminescence, and a peak in the photoconductivity near 1.84 eV. The peak corresponds to the A exciton, which is the lowest energy exciton in monolayers. The A and higherenergy B excitons are excited at a direct transition from a valence band split into two branches by spin-orbit coupling. The direct-to-indirect gap evolution is evident from the quenching of the photoluminescence for films thicker than a monolayer. The first electronic structure calculations on MoS<sub>2</sub> nanotubes predicted bandgap trends, strain and curvature, and other signatures of chirality.<sup>13</sup> Those calculations and subsequent experiments have shown that the exciton energies lie below those of the corresponding bulk material, and the A exciton shifts with tube diameter because of the changing strain. Single wall MoS<sub>2</sub> and WS2 nanotubes with zigzag structure exhibit direct gap transitions, whereas tubes with armchair structure have an indirect transition.13

But unlike their flake counterparts, multilayer MoS<sub>2</sub> tubes emit light.<sup>14</sup> Their emission includes photoluminescence (PL) from both direct and indirect excitons and is induced by various symmetry-breaking effects. In PL measurements on multiwall MoS<sub>2</sub> tubes, the A exciton energy is below that of a flake, and its shape and intensity depend on whether the tube has a circular cross section or is somewhat flattened. Additionally, optical whispering gallery modes travel around the rim of a nanotube, as shown in the inset of figure 3a. Excitons couple with those modes to form quasiparticles known as polaritons. Those polaritons lead to a series of peaks on the low-energy side of the A exciton's PL, as shown in figure 3a for experiment and simulations. Each peak corresponds to a polariton formed by an optical mode with a different angular-momentum quantum number, which is indicated over the peak.

The strength of the interaction between the exciton and

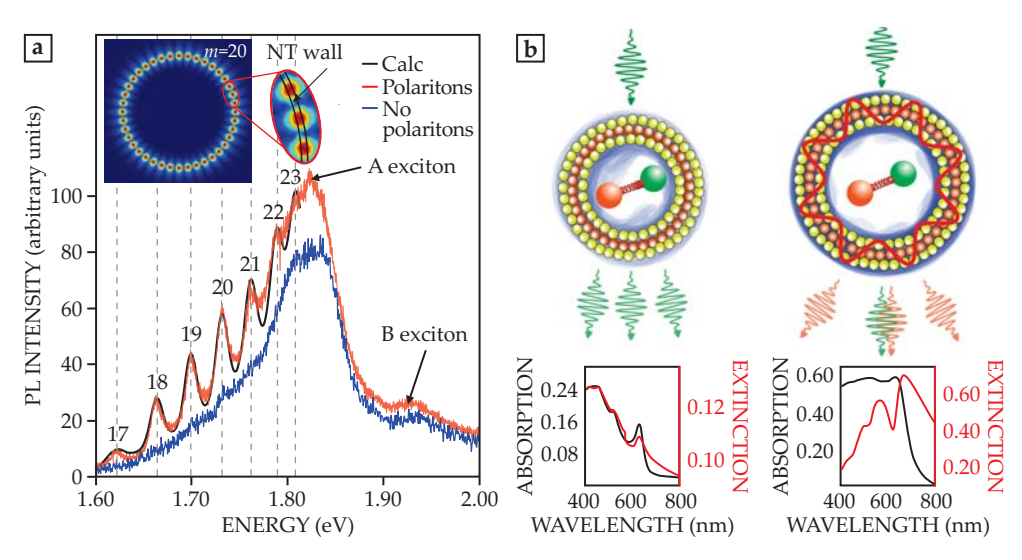


FIGURE 3. EXCITONS AND POLARITONS DICTATE A NANOTUBE'S OPTICAL PROPERTIES. (a) Molybdenum disulfide nanotubes host whispering gallery modes, as shown as a simulation in the inset. Those modes have angular momentum characterized by quantum number m. The tube's excitons can couple with optical modes to form polaritons, and those polaritons introduce a series of peaks present in the photoluminescence (PL), as shown in experimental results (red) and calculations (black), but absent in a typical PL spectrum (blue). The peaks correspond to different values of m. (Adapted from ref. 14.) (b) A small (< 60 nm, left) and a large (> 80 nm, right) nanotube respond differently to optical excitation. Narrow tubes display simple excitonic absorption (green wavy arrows) that results in almost matching absorbance (black) and extinction (red) graphs. The polaritons in large-diameter tubes strongly scatter light (red wavy arrows) alongside the weaker excitonic absorption. The resulting extinction and net absorption spectra are quite different from each other. (Courtesy of Sudarson S. Sinha; adapted from ref. 15.)

optical mode is described by a quantity known as Rabi splitting. In the strong coupling limit with Rabi splitting of 400 meV, the exciton splits the polariton mode into upper and lower branches with an energy difference given by the splitting. Complementary work on WS $_2$  tubes demonstrates coupling with Rabi splitting of 270–330 meV, $^{15}$  much larger than III–V compounds such as gallium arsenide.

The optical extinction and absorption of WS<sub>2</sub> nanotubes with different average diameters show that only some nanotubes host polaritons. A centrifuge tube loaded with pristine powder and run at different speeds produced batches of nanotubes with different average diameter between 30 nm and 150 nm. <sup>16</sup> WS<sub>2</sub> nanotubes with diameter smaller than 60 nm cannot confine the light, and as a result, they display purely excitonic absorption and extinction, as shown on the left side of figure 3b. However, nanotubes of diameter 80 nm and larger exhibit strong coupling of the A and B excitons with the optical cavity modes confined in the nanotube. That coupling leads to dips in the extinction spectra at energies very close to the position of the A and B excitons.

Additional evidence for polaritonic behavior comes from transient absorption and extinction spectra. <sup>15</sup> For large-diameter WS<sub>2</sub> tubes, two dips in the transmission at 1.88 eV and 2.25 eV appear, which are blueshifted by 40 meV during the first 30 ps.

For the shortest delay, the energies of the photobleaching dips almost coincide with the first and second polaritonic peaks of the extinction spectrum. For small-diameter nanotubes, the photobleaching dips nearly align with the A and B exciton peaks and reveal a relatively small 10 meV blueshift—more like TMDC flakes, which don't blueshift. Previously, strong coupling effects appeared mostly in hybrid nanomaterials—for example, plasmonic light-scattering from a cadmium selenide quantum dot fused to a gold nanoparticle. The strong coupling in WS<sub>2</sub> nanotubes is a manifestation of their quasi-1D character and high refraction coefficient, which can confine the optical cavity modes required for polariton formation.

### Superconductivity

 $WS_2$  nanotubes are ordinarily semiconducting, but when highly doped with electrons, they turn metallic and even superconducting. In an ionic-gating device, the nanotube's doping is controlled by the voltage applied to a droplet of potassium perchlorate/polyethylene glycol electrolyte, <sup>17</sup> as shown in figure 4a. The voltage drives potassium to intercalate in the nanotube, where the ions donate electrons until a heavily doped semiconducting nanotube becomes highly metallic. When that nanotube is cooled to cryogenic temperatures, it becomes superconducting, with critical temperature of 5.8 K.

A large-enough magnetic field applied parallel to the tube axis suppresses the superconductivity, and the normal-state resistance is restored. On the way back to the normal state, the resistance shows small oscillations as a function of magnetic field. Figure 4b shows the extracted signals, which are known as Little–Parks oscillations of the supercurrent. The phenomenon is exclusive to cylindrical superconductors, and the oscillation period is related to the effective tube diameter—in the current case estimated at 80 nm, which is consistent with that obtained from atomic force microscopy measurements.

How does the chiral structure of a WS<sub>2</sub> nanotube influence transport phenomena? Rightward and leftward currents differ by 1-2% under a magnetic field parallel to the tube's axis. That directional dependence, called nonreciprocity, arises from the interaction of the magnetic field produced by the current and the applied magnetic field. When the current is fed through a chiral object, it consists of three components: parallel to the tube, along the circumference, and chiral. The chiral component produces a magnetic field parallel to the tube. When an external magnetic field is applied parallel to the tube, the magnetic field produced by the current is either parallel or antiparallel to the external magnetic field. The result is nonreciprocity in the resistance.

The nonreciprocal signal is sensitively detected by alternating-current resistance measurements. When a current with frequency  $\omega$  is applied to a nanotube, the output voltage alters

with frequency  $\omega$  and also  $2\omega$ . The  $2\omega$  component  $\tilde{V}^{2\omega}$  is a measure of the nonreciprocity, and that response is dramatically enhanced in the superconducting state. The Little–Parks effect appears also in the second harmonic resistance signal. The simultaneous observation of the Little–Parks oscillations and nonreciprocal responses provides additional, unambiguous evidence that superconductivity occurs in the chiral tubes rather than in impurities or residual objects inside the tubes.

An 80 nm WS<sub>2</sub> tube, which is much thicker than a single-walled carbon nanotube, isn't expected to have quantized energy levels. And the system's low electrical mobility hinders the observation of chirality effects in the normal state. But once superconductivity sets in, phenomena arising from the intrinsic structure of the chiral tubes become visible because of the high coherence of the current flow. For example, another study found that the critical temperature decreased with decreasing tube diameter <sup>17</sup>

#### **Bulk photovoltaic effect**

 $WS_2$  nanotubes have a structural feature that is absent in carbon nanotubes: polarity, which emerges because two of the mirror symmetries in 2D  $WS_2$  are lost when it's rolled up. That polar nature leads to photovoltaic properties without the usual p-n or Schottky junctions. In the normal photovoltaic effect, shown schematically in figure 5a, light generates electron–hole pairs, which are driven away from each other by the local electric field at a junction. The resulting electricity is the basis for commercial solar cells. But materials with broken inversion symmetry can have the photovoltaic effect without a junction. A conventional interpretation of the effect, known as the bulk photovoltaic effect, is that photoexcited electrons and holes are separated by the internal electric field in polar materials, including ferroelectrics. Many experimental observations contradict such a simple view, so a new mechanism, shift current, has been proposed.

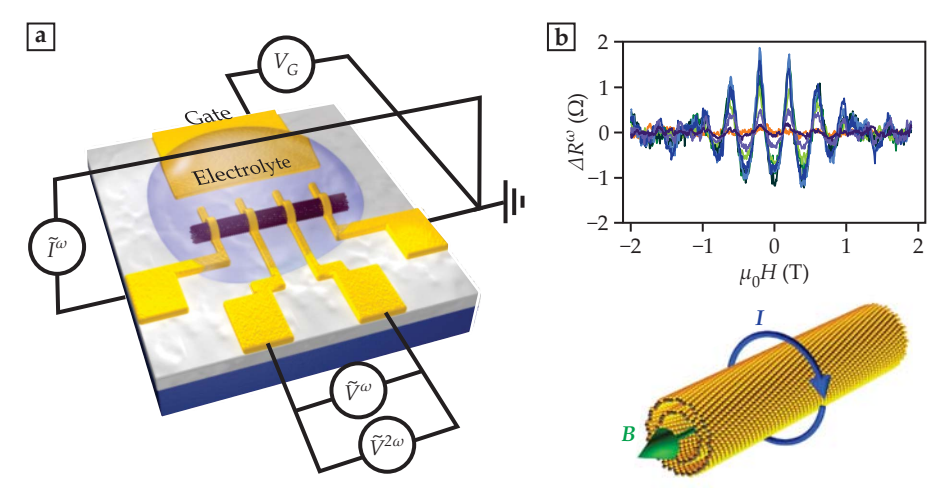
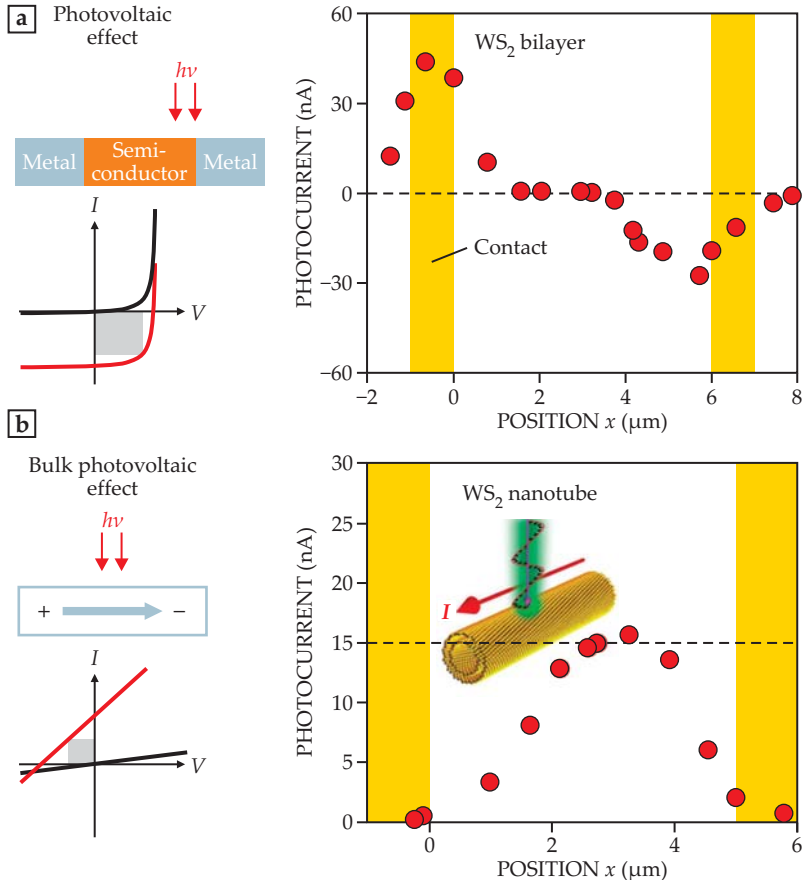


**FIGURE 4. HIGHLY DOPED NANOTUBES BECOME SUPERCONDUCTING. (a)** In a device, a nanotube (purple cylinder) is doped by a voltage  $V_{\rm G}$  applied to an electrolyte droplet. The current  $\widetilde{I}^{\omega}$  and the output voltage components with frequency  $\omega$  ( $\widetilde{V}^{\omega}$ ) and  $2\omega$  ( $\widetilde{V}^{2\omega}$ ) are probed by gold contacts (yellow). At high doping and at a temperature below 5.8 K, the nanotube becomes superconducting. **(b)** Under an applied magnetic field B with a radial current I, a nanotube's differential resistance  $\Delta R^{\omega}$  fluctuates with the auxiliary field B. That response, known as Little–Parks oscillations, arises from the tube's cylindrical shape and is related to its diameter. (Adapted from ref. 17.)

#### **NANOTUBES**



The bulk photovoltaic effect is also expected in 2D monolayers of the WS<sub>2</sub> polymorph that has broken inversion symmetry.

To compare the photovoltaic effect and the bulk photovoltaic effect, bilayer WS<sub>2</sub> and WS<sub>2</sub> nanotubes are both irradiated by a laser spot, which scans the sample. The WS<sub>2</sub> bilayer (see figure 5a) has a photocurrent signal with opposite signs when the laser hits the two gold–WS<sub>2</sub> contacts. In contrast, the photocurrent in the WS<sub>2</sub> nanotubes peaks when the laser is between the gold contacts, as shown in figure 5b, and that indicates the bulk photovoltaic effect.<sup>18</sup> The photocurrent's dependence on the light intensity supports the recently proposed shift-current mechanism, which is the result of the real-space shift of the photoexcited conduction and valence Bloch electrons by a topological quantity, the Berry phase.

The photocurrent density generated in WS<sub>2</sub> nanotubes is several orders of magnitude larger than that of bulk ferroelectric materials. A large photocurrent response that doesn't require an energy-sapping electric field makes nanotubes promising for applications such as IR sensors. The higher efficiency offered by their 1D character and nanoscale dimensions could also prove useful for photovoltaic and nanophotonics devices, field-effect transistors, *p-n* junctions, thermoelectric generators, and optical resonators with *Q*-factors on the order of several hundred, to name a few. Furthermore, the strong catalytic activity of bulk MoS<sub>2</sub> and WS<sub>2</sub> suggests that their nanotube counterparts could work in nanocatalysis and advanced hydrogen storage platforms.

Nanotubes are also a platform for more fundamental exploration of physical properties in 1D without the issue of dangling bonds and defects common in nanowires. Those applications, studies, and more will become practical as new synthesis

# FIGURE 5. THE PHOTOVOLTAIC EFFECT, CONVENTIONAL AND BULK. (a) In the

photovoltaic effect, light with energy hv, in terms of Planck's constant h and frequency v, excites a semiconductor with two metal contacts (left). Photoexcited carriers are separated by the electric field at the junction between the metal and semiconductor. The black and red I-V curves are for a single Schottky junction in the dark and under light, respectively, and the area of the gray box represents the power produced. In a bilayer WS<sub>2</sub>-based device, the photocurrent becomes nonzero only when the laser spot, at position x, is on the gold contacts, as expected for the photovoltaic effect. (b) A polar material usually exhibits a nearly linear I-V curve (black, on left), whereas it shows photocurrent (red) when irradiated by a laser. As a result, a polar WS<sub>2</sub> nanotube device, shown on the right, has a photocurrent at zero bias that reaches a maximum when the laser spot illuminates the center of the device away from the contacts. (Adapted from ref. 18.)

techniques work to produce  $MoS_2$  and  $WS_2$  nanotubes in both high quality and substantial amounts, beyond the current maximum rate of 100 g/day.

We acknowledge support by the US Department of Energy, Office of Basic Energy Sciences, materials science division, grant no. DE-FG02-01ER45885 (Musfeldt); by JSPS KAKENHI grant no. JP19H05602 and the A3 Foresight Program (Iwasa); and by Israel Science Foundation grant nos. 339/18 and 120924, the Perlman Family Foundation, and Kimmel Center for Nanoscale Science grant no. 43535000350000 (Tenne).

#### REFERENCES

- 1. R. Tenne et al., *Nature* **360**, 444 (1992); Y. Feldman et al., *Science* **267**, 222 (1995); N. G. Chopra et al., *Science* **269**, 966 (1995).
- 2. L. S. Panchakarla et al., J. Phys. Chem. Lett. 5, 3724 (2014).
- I. Kaplan-Ashiri et al., Proc. Natl. Acad. Sci. USA 103, 523 (2006);
   D.-M. Tang et al., Nano Lett. 13, 1034 (2013).
- O. Tevet et al., Proc. Natl. Acad. Sci. USA 108, 19901 (2011); I. Lahouij et al., Tribol. Lett. 42, 133 (2011); D. Maharaj, B. Bhushan, Tribol. Lett. 49, 323 (2013).
- 5. F. Dassenoy, Tribol. Online 14, 237 (2019).
- 6. O. Goldbart et al., Proc. Natl. Acad. Sci. USA 113, 13624 (2016).
- 7. K. R. O'Neal et al., Nano Lett. 16, 993 (2016).
- 8. M. Ghorbani-Asl et al., Sci. Rep. 3, 2961 (2013).
- 9. O. Grinberg et al., Phys. Chem. Chem. Phys. 19, 18443 (2017).
- J. L. Verble, T. J. Wietling, P. R. Reed, Solid State Commun. 11, 941 (1972).
- J.-W. Jiang, B.-S. Wang, T. Rabczuk, Nanotechnology 25, 105706 (2014).
- 12. M. Staiger et al., Phys. Rev. B 86, 165423 (2012).
- 13. G. Seifert et al., Phys. Rev. Lett. 85, 146 (2000).
- D. R. Kazanov et al., Appl. Phys. Lett. 113, 101106 (2018); Y. J. Zhang et al., 2D Mater. 5, 035002 (2018).
- L. Yadgarov et al., Phys. Chem. Chem. Phys. 20, 20812 (2018); S. S. Sinha et al., Small 16, 1904390 (2020).
- 16. Y. Yomogida et al., ACS Omega 3, 8932 (2018).
- 17. F. Qin et al., *Nat. Commun.* **8**, 14465 (2017); F. Qin et al., *Nano Lett.* **18**, 6789 (2018).
- 18. Y. J. Zhang et al., Nature 570, 349 (2019).